Available online at www.sciencedirect.com
SCIENCE DIRECT®
Journal of Computational Physics 197 (2004) 585–609
JOURNAL OF COMPUTATIONAL PHYSICS
www.elsevier.com/locate/jcp

On the preservation of phase space structure under multisymplectic discretization

A.L. Islas [a], C.M. Schober [b,*]

[a] Department of Mathematics and Statistics, Old Dominion University, Norfolk, VA 23529, USA
[b] Department of Mathematics, University of Central Florida, P.O. Box 161364, Orlando, FL 32816, USA

Received 23 June 2003; received in revised form 5 December 2003; accepted 5 December 2003
Available online 22 January 2004

Abstract

In this paper we explore the local and global properties of multisymplectic discretizations based on finite differences and Fourier spectral approximations. Multisymplectic (MS) schemes are developed for two benchmark nonlinear wave equations, the sine-Gordon and nonlinear Schrödinger equations. We examine the implications of preserving the MS structure under discretization on the numerical scheme's ability to preserve phase space structure, as measured by the nonlinear spectrum of the governing equation. We find that the benefits of multisymplectic integrators include improved resolution of the local conservation laws, dynamical invariants and complicated phase space structures.

PACS: 02.30.Ik; 02.30.Jr; 02.60.Lj

Keywords: Multisymplectic integrators; Nonlinear spectral diagnostics; Nonlinear Schrödinger equation; Sine-Gordon equation

1. Introduction

Multisymplectic integrators, i.e. numerical schemes which exactly preserve a discrete space–time symplectic structure, are a new approach to solving Hamiltonian PDEs [3,4,14]. Since the use of multisymplectic integrators is a relatively recent development, to date much of the literature has been devoted to establishing that various discretization methods (e.g. Fourier spectral, Gauss–Legendre collocation, finite volume) have subclasses which are multisymplectic [3,4,9,10]. Multisymplectic variational integrators based on Hermite type finite element bases have also been developed [13]. However, a thorough analysis of the local and global properties of multisymplectic integrators has yet to be carried out.

Preservation of the multisymplectic structure by a numerical scheme does not imply preservation of other dynamical invariants of the system such as the local conservation laws or of global invariants which

* Corresponding author.
E-mail addresses: islas@math.odu.edu (A.L. Islas), cschober@mail.ucf.edu (C.M. Schober).

0021-9991/$ - see front matter
doi:10.1016/j.jcp.2003.12.010

determine the phase space structure. A question that immediately arises then is, to what extent are the other invariants of the system preserved? In long time studies of low-dimensional Hamiltonian ODEs, symplectic integrators capture global phase space structures better than standard integrators which allow the actions to drift [8]. Thus it is reasonable to expect that this behavior might carry over to multisymplectic discretizations of Hamiltonian PDEs.

Recent numerical experiments using multisymplectic (MS) integrators to solve nonlinear wave equations suggest that the local conservation laws are preserved very well, although not exactly, over long times [3,10]. Specifically, using a MS finite-difference discretization of the nonlinear Schrödinger (NLS) equation, our numerical studies demonstrate that the local energy and momentum conservation laws are preserved far better than expected, given the order of the scheme. In addition, several global invariants are preserved within roundoff (see Section 5).

Nonlinear wave equations such as the NLS and sine-Gordon (SG) equations can have a complicated phase space structure, depending on the type of boundary conditions considered. In this case, MS finite-difference schemes can have difficulty in resolving spatial structures in very sensitive regimes. Even so, we find that the local conservation laws are important indicators of spatial discretization errors which can corrupt the solution and, as such, provide additional insight into the qualitative behavior of the numerical scheme. Alternatively, spectral methods have proven to be highly effective methods for solving evolution equations. As the number N of space grid points increases, errors typically decay at an exponential rate rather than at polynomial rates obtained with finite-difference approximations [7]. Not surprisingly, MS spectral methods outperform MS discretizations based on finite differences and are the method of choice for sensitive regimes and multi-dimensional problems [12].

In this paper we examine the preservation of phase space structures by MS spectral methods for two benchmark problems, the NLS and SG equations. These equations are completely integrable (integrability is established using a Lax pair, Eq. (15)) and their phase space geometry is specified in terms of the nonlinear spectrum of the spatial operator of the associated Lax pair. We implement MS and non-symplectic spectral methods for the NLS and SG equations and exploit the nonlinear spectrum as a basis for comparing the effectiveness of the integrators in capturing the phase space dynamics. The relevant quantities to monitor are the periodic/antiperiodic eigenvalues of the spectral problem. These eigenvalues are the spectral representation of the action variables and are directly related to the geometry of the phase space. We find that the nonlinear spectrum is a particularly insightful tool for analyzing the qualitative behavior of the numerical schemes and we advocate its general use in further studies of geometric integrators. Other classes of PDE integrators can be tested on integrable systems, using the nonlinear spectrum as a diagnostic to address various questions on phase space preservation (e.g. how well stable tori are preserved, what is the width of chaotic layer that appears when unstable tori break up, etc.).

Significantly, we show that MS spectral methods provide an improved resolution of the LCLs, of the nonlinear spectrum and phase space structure, and the qualitative features of the solutions, when compared with non-symplectic spectral integrators. Consequently, we find that conservation of multisymplecticity by a numerical scheme does result in an improved preservation of the phase space structure. This is the first examination of the implications, in terms of preservation of the phase space structure and the nonlinear spectrum, of preserving the MS structure under discretization and provides a deeper understanding of the local and global properties of MS integrators.

The paper is organized as follows: in Section 2 we recall the MS formulation of Hamiltonian PDEs and of the NLS and SG equations. We present a description of their phase space geometry in terms of the associated nonlinear spectral theory. We provide the elements of the integrable theory which are relevant for interpreting the ability of the numerical schemes to preserve the phase space structure. In Section 3 we introduce the multisymplectic box scheme, apply it to the NLS, and discuss it's properties. In Section 4 we establish that spectral discretizations yield another class of multisymplectic integrators and discuss their conservation properties. We prove that if $S(z)$ is quadratic, then the MS spectral scheme conserves the

LCLs exactly. We obtain MS spectral discretizations for the NLS and SG equations. The numerical experiments, which illustrate the remarkable behavior of MS schemes, are discussed in Section 5. In particular, we examine how the preservation of the LCLs and the phase space structure depends upon the multisymplectic property of the numerical scheme.

2. Background

2.1. Multisymplectic formulation of Hamiltonian PDEs

A Hamiltonian PDE (in the "1 + 1" case) is said to be *multisymplectic* if it can be written as

$$\boldsymbol{M}z_t + \boldsymbol{K}z_x = \nabla_z S, \quad z \in \mathbb{R}^d, \tag{1}$$

where $\boldsymbol{M}, \boldsymbol{K} \in \mathbb{R}^{d\times d}$ are skew-symmetric matrices and $S : \mathbb{R}^d \to \mathbb{R}$ is a smooth function of the state variable z [1,3]. The variational equation associated with (1) is given by

$$\boldsymbol{M}\,\mathrm{d}z_t + \boldsymbol{K}\,\mathrm{d}z_x = \boldsymbol{S}_{zz}\,\mathrm{d}z. \tag{2}$$

The term multisymplectic is applied to system (1) in the sense that associated with $\boldsymbol{M}$ and $\boldsymbol{K}$ are the two forms

$$\omega = \frac{1}{2}(\mathrm{d}z \wedge \boldsymbol{M}\,\mathrm{d}z), \quad \kappa = \frac{1}{2}(\mathrm{d}z \wedge \boldsymbol{K}\,\mathrm{d}z), \tag{3}$$

which define a space–time symplectic structure (i.e. symplectic with respect to more than one independent variable).

Any system of the form (1) satisfies conservation of symplecticity. Let $\mathrm{d}z$ be a solution of the variational equation (2). Then it can be shown that ω and κ, as defined in (3), satisfy the multisymplectic conservation law (MSCL)

$$\partial_t \omega + \partial_x \kappa = 0. \tag{4}$$

Symplecticity is a global property for Hamiltonian ODEs; in contrast, it is a local property for Hamiltonian PDEs. The MSCL (4) expresses the fact that symplecticity can vary over the spatial domain and from time to time. This variation is not arbitrary as the changes in time are exactly compensated by changes in space.

An important consequence of multisymplecticity is that when the Hamiltonian S is independent of x and t, the PDE has local energy and momentum conservation laws (LECL and LMCL)

$$\begin{aligned} &E_t + F_x = 0, \quad E = S - \frac{1}{2}z^T\boldsymbol{K}z_x, \quad F = \frac{1}{2}z^T\boldsymbol{K}z_t, \\ &I_t + G_x = 0, \quad G = S - \frac{1}{2}z^T\boldsymbol{M}z_t, \quad I = \frac{1}{2}z^T\boldsymbol{M}z_x. \end{aligned} \tag{5}$$

Note that S itself is not preserved. For periodic boundary conditions, the local conservation laws (LCLs) can be integrated in x to obtain global conservation of energy momentum.

2.1.1. Multisymplectic formulation of the model equations

The focusing one-dimensional nonlinear Schrödinger (NLS) equation,

$$\mathrm{i}u_t + u_{xx} + 2|u|^2 u = 0, \tag{6}$$

can be written in multisymplectic form by letting $u = p + \mathrm{i}q$ and introducing the new variables $v = p_x, w = q_x$ [1]. Separating (6) into real and imaginary parts, we obtain the system

$$\begin{aligned} &q_t - v_x = 2\left(p^2 + q^2\right)p, \\ &-p_t - w_x = 2\left(p^2 + q^2\right)q, \\ &p_x = v, \\ &q_x = w, \end{aligned} \tag{7}$$

which is equivalent to the multisymplectic form (1) for the NLS equation with

$$z = \begin{pmatrix} p \\ q \\ v \\ w \end{pmatrix}, \quad \boldsymbol{M} = \begin{pmatrix} 0 & 1 & 0 & 0 \\ -1 & 0 & 0 & 0 \\ 0 & 0 & 0 & 0 \\ 0 & 0 & 0 & 0 \end{pmatrix}, \quad \boldsymbol{K} = \begin{pmatrix} 0 & 0 & -1 & 0 \\ 0 & 0 & 0 & -1 \\ 1 & 0 & 0 & 0 \\ 0 & 1 & 0 & 0 \end{pmatrix},$$

and Hamiltonian $S = \frac{1}{2}\left[\left(p^2 + q^2\right)^2 + v^2 + w^2\right]$.

Implementing relations (5) for the NLS equation yields the LECL and LMCL laws

$$\begin{aligned} &E_t + F_x = 0, \quad E = \frac{1}{2}\left[\left(p^2 + q^2\right)^2 - v^2 - w^2\right], \;\; F = vp_t + wq_t, \\ &I_t + G_x = 0, \quad I = pw - qv, \;\; G = \left(p^2 + q^2\right)^2 + v^2 + w^2 - (pq_t - p_t q). \end{aligned} \tag{8}$$

Additionally we have a norm conservation law for the NLS equation

$$N_t + M_x = 0, \quad N = \frac{1}{2}\left(p^2 + q^2\right), \;\; M = qv - pw. \tag{9}$$

These three equations, when integrated with respect to x, yield the classical global conservation of energy (the Hamiltonian), momentum and norm defined as

$$\frac{\mathrm{d}}{\mathrm{d}t}\mathscr{E}(z) = 0, \quad \frac{\mathrm{d}}{\mathrm{d}t}\mathscr{I}(z) = 0, \quad \frac{\mathrm{d}}{\mathrm{d}t}\mathscr{N}(z) = 0, \tag{10}$$

where $\mathscr{E}(z) = \int_0^L E(z)\,\mathrm{d}x$, $\mathscr{I}(z) = \int_0^L I(z)\,\mathrm{d}x$, $\mathscr{N}(z) = \int_0^L N(z)\,\mathrm{d}x$.

The second nonlinear wave equation that we consider is the sine-Gordon equation

$$u_{tt} - u_{xx} + \sin u = 0. \tag{11}$$

By introducing the variables $v = u_t$ and $w = u_x$, we obtain the system of equations

$$\begin{aligned} &-v_t + w_x = \sin u, \\ &u_t = v, \\ &-u_x = -w. \end{aligned} \tag{12}$$

System (12) can be written in standard multisymplectic form with

$$\boldsymbol{M} = \begin{pmatrix} 0 & -1 & 0 \\ 1 & 0 & 0 \\ 0 & 0 & 0 \end{pmatrix}, \quad \boldsymbol{K} = \begin{pmatrix} 0 & 0 & 1 \\ 0 & 0 & 0 \\ -1 & 0 & 0 \end{pmatrix}, \quad S = \frac{1}{2}\left(v^2 - w^2\right) - \cos u, \tag{13}$$

and $z = (u, v, w)^{\mathrm{T}}$. The local energy and momentum conservation laws are simplified to

$$\begin{aligned} &E_t + F_x = 0, \quad E = \frac{1}{2}(v^2 + w^2) - \cos u, \;\; F = -vw, \\ &I_t + G_x = 0, \quad I = -vw, \;\; G = \frac{1}{2}(v^2 + w^2) + \cos u. \end{aligned} \tag{14}$$

The multisymplectic form of the sine-Gordon equation in Eqs. (11)–(13) has certain disadvantages. Firstly the left-hand side ($M\partial_t + K\partial_x$) has an infinite-dimensional kernel; secondly, there is a hidden constraint which is not represented; and thirdly, the matrices M and K are both degenerate. It is now known that this multisymplectic structure can be improved [2]. Starting with the canonical form of the Lagrangian for the sine-Gordon equation (11)

$$\mathscr{L} = \int\int L(u, u_t, u_x)\mathrm{d}x \wedge \mathrm{d}t, \quad L(u, u_t, u_x) = u_t^2 - u_x^2 - 1 + \cos(u),$$

the Legendre transform can be used to generate a new Hamiltonian functional

$$S(u, v, w) = vu_t + wu_x - L = v^2 - w^2 + 1 - \cos(u),$$

and a new Lagrangian for the system

$$\mathscr{L} = \int\int L(u, v, w)\mathrm{d}x \wedge \mathrm{d}t, \quad L(u, v, w) = vu_t + wu_x - S(u, v, w).$$

The governing equations are given by

$$0 = L_u = -v_t - w_x - S_u,$$

$$0 = L_v = u_t - S_v,$$

$$0 = L_w = u_x - S_w,$$

using standard fixed endpoint conditions for the variations. These are the equations used in Eq. (12) (modulo the sign change on w).

To improve this structure, observe that v and w satisfy the constraint $w_t + v_x = 0$. Adding this constraint to the Lagrangian with Lagrange multiplier p, we obtain

$$\mathscr{L} = \int\int \tilde{L}(u, v, w, p)\mathrm{d}x \wedge \mathrm{d}t, \quad \tilde{L}(u, v, w, p) = L(u, v, w) + p(w_t + v_x).$$

The governing equations are now

$$0 = \tilde{L}_u = -v_t - w_x - S_u,$$

$$0 = \tilde{L}_v = u_t - S_v - p_x,$$

$$0 = \tilde{L}_w = u_x - S_w - p_t,$$

$$0 = \tilde{L}_p = w_t + v_x,$$

or in multisymplectic canonical form

$$\begin{pmatrix} 0 & -1 & 0 & 0 \\ 1 & 0 & 0 & 0 \\ 0 & 0 & 0 & -1 \\ 0 & 0 & 1 & 0 \end{pmatrix} \begin{pmatrix} u \\ v \\ w \\ p \end{pmatrix}_t + \begin{pmatrix} 0 & 0 & -1 & 0 \\ 0 & 0 & 0 & -1 \\ 1 & 0 & 0 & 0 \\ 0 & 1 & 0 & 0 \end{pmatrix} \begin{pmatrix} u \\ v \\ w \\ p \end{pmatrix}_x = \begin{pmatrix} \sin(u) \\ v \\ -w \\ 0 \end{pmatrix}.$$

2.2. Integrable structure of the model equations

The integrability of the NLS equation (6) is established using the associated linear systems

$$\mathscr{L}^{(x)}\phi = 0, \quad \mathscr{L}^{(t)}\phi = 0, \tag{15}$$

(the so-called Lax pair), where

$$\mathscr{L}^{(x)} = \begin{pmatrix} \frac{\mathrm{d}}{\mathrm{d}x} + \mathrm{i}\lambda & -u \\ u^* & \frac{\mathrm{d}}{\mathrm{d}x} - \mathrm{i}\lambda \end{pmatrix}, \quad \mathscr{L}^{(t)} = \begin{pmatrix} \frac{\mathrm{d}}{\mathrm{d}t} + \mathrm{i}[2\lambda^2 - |u|^2] & -2\lambda u - \mathrm{i}u_x \\ 2\lambda u^* - \mathrm{i}u_x^* & \frac{\mathrm{d}}{\mathrm{d}t} - \mathrm{i}[2\lambda^2 - |u|^2] \end{pmatrix}$$

and λ is the spectral parameter. This system has a common solution $\phi(x,t;\lambda)$, provided the coefficient $u(x,t)$ satisfies Eq. (6).

Every NLS solution $u(x,t)$, as well as the NLS phase space, is characterized by the spectrum $\sigma(u) := \{\lambda \in \mathbb{C} \,|\, \mathscr{L}^{(x)}\boldsymbol{v} = 0,\ |\boldsymbol{v}| \text{ bounded } \forall x\}$ of the associated linear operator $\mathscr{L}^{(x)}$ [5]. For periodic boundary conditions $u(x+L,t) = u(x,t)$, the spectrum is obtained using Floquet theory. The spectrum of u can be written in terms of the transfer matrix $M(x+L;u,\lambda)$ across a period, where $M(x;u,\lambda)$ denotes a fundamental solution matrix of the Lax pair (15). Introducing the Floquet discriminant $\Delta(u,\lambda) := \mathrm{Trace}[M(x+L;u,\lambda)]$, one obtains

$$\sigma(u) := \{\lambda \in \mathbb{C} \,|\, \Delta(u,\lambda) \in \mathbb{R}, -2 \leqslant \Delta(u,\lambda) \leqslant 2\}. \tag{16}$$

The Floquet discriminant is analytic in both its arguments. Moreover, for a fixed λ, Δ is invariant along solutions of the NLS equation: $(\mathrm{d}\Delta/\mathrm{d}t)(u,\lambda) = 0$. Since Δ is invariant and the functionals $\Delta(u,\lambda)$, $\Delta(u,\lambda')$ are pairwise in involution, Δ provides an infinite number of commuting invariants for the NLS equation.

The Floquet spectrum (16) of a typical solution consists of bands of continuous spectrum with simple periodic eigenvalues as endpoints (for example, finite-genus solutions are those with a finite number of bands of continuous spectrum). The distinguished points of the periodic/antiperiodic spectrum are: (a) simple critical points $\{\lambda_j^{\mathrm{s}} \,|\, \Delta(\lambda,u) = \pm 2, \mathrm{d}\Delta/\mathrm{d}\lambda \neq 0\}$ and (b) double points $\{\lambda_j^{\mathrm{d}} \,|\, \Delta(\lambda,u) = \pm 2, \mathrm{d}\Delta/\mathrm{d}\lambda = 0, \mathrm{d}^2\Delta/\mathrm{d}\lambda^2 \neq 0\}$.

The periodic/antiperiodic spectrum provides the actions in an action-angle description of the system. The values of these actions fix a particular level set. Let λ denote the spectrum associated with the potential u. The level set defined by u is then given by, $\mathscr{M}_u \equiv \{v \,|\, \Delta(v,\lambda) = \Delta(u,\lambda), \lambda \in \mathbb{C}\}$. Typically, $\mathscr{M}_u$ is an infinite-dimensional stable torus. However, the NLS phase space also contains degenerate tori which may be unstable. If a torus is unstable, its invariant level set consists of the torus and an orbit homoclinic to the torus. These invariant level sets, consisting of an unstable component, are represented, in general, by complex double points in the spectrum. A complete and detailed description of the NLS phase space structure is provided in [5].

The simplest example is the plane wave solution $u(x,t) = a\mathrm{e}^{2\mathrm{i}a^2 t}$. The discriminant is readily computed to be

$$\Delta(a,\lambda) = 2\cos(\sqrt{a^2+\lambda^2}L). \tag{17}$$

The associated Floquet spectrum consists of the continuous bands $\mathbb{R} \bigcup [-\mathrm{i}a, \mathrm{i}a]$, and a discrete part containing the simple periodic/antiperiodic eigenvalues $\pm\mathrm{i}a$, and the infinite sequence of double points

$$\lambda_j^2 = \left(\frac{\mathrm{j}\pi}{L}\right)^2 - a^2, \quad j \in \mathbb{Z}. \tag{18}$$

Of these, if $[aL/\pi] = M$ (where $[p]$ = largest integer $\leqslant p$, $p > 0$), $2M$ are complex (pure imaginary) double points, while the remaining λ_j's for $|\mathrm{j}| > M$ are real. The initial conditions used in the numerical study are small finite-genus perturbations of unstable plane waves with one or two unstable modes (the "one-complex double point regime"); this is the case, provided $[aL/\pi] = 1, 2$. The condition for complex double points is exactly the same as the condition for the solution to be linearly unstable.

The Floquet theory for the SG equation and a description of its phase space geometry in terms of the nonlinear spectrum is formally analogous to that of NLS. Here we simply provide the spatial part of the Lax pair for the SG equation [6]

$$\mathscr{L}^{(x)} = \left[\boldsymbol{A}\frac{\mathrm{d}}{\mathrm{d}x} + \frac{\mathrm{i}}{4}\boldsymbol{B}(u_x + u_t) + \frac{1}{16\lambda}\boldsymbol{C} - \lambda\boldsymbol{I}\right],$$

where $\boldsymbol{I}$ is the identity matrix, u is the potential, $\lambda \in \mathbb{C}$ is the spectral parameter, and

$$\boldsymbol{A} = \begin{pmatrix} 0 & -1 \\ 1 & 0 \end{pmatrix}, \quad \boldsymbol{B} = \begin{pmatrix} 0 & 1 \\ 1 & 0 \end{pmatrix}, \quad \boldsymbol{C} = \begin{pmatrix} \mathrm{e}^{\mathrm{i}u} & 0 \\ 0 & \mathrm{e}^{-\mathrm{i}u} \end{pmatrix}.$$

As an example, consider the solution $u(x,t) = (\pi, 0)$. The Floquet discriminant is given by $\Delta(\boldsymbol{u}, \lambda) = 2\cos(\lambda + \frac{1}{16\lambda})L$ and the spectrum by $\sigma(\mathscr{L}) = \mathbb{R}\bigcup(|\lambda|^2 = 1/16)$. The periodic spectrum is located at

$$\lambda_j = \frac{1}{2}\left[\frac{\mathrm{j}\pi}{L} \pm \sqrt{\frac{\mathrm{j}^2\pi^2}{L^2} - \frac{1}{4}}\right], \quad j \in \mathbb{Z}.$$

Each of these points is a double point embedded in the continuous spectrum and becomes complex if $0 \leqslant (2\pi\mathrm{j}/L)^2 < 1$. As for the NLS equation, the condition for complex double points is exactly the same as the condition for unstable modes.

3. Multisymplectic finite-difference schemes

Multisymplectic discretizations are numerical schemes for approximating (1) which preserve a discrete version of the multisymplectic conservation law (4). That is, if the discretization of the multisymplectic PDE and its conservation law are written schematically as

$$\boldsymbol{M}\partial_t^{i,j} z_i^j + \boldsymbol{K}\partial_x^{i,j} z_i^j = (\nabla_z S(z_i^j))_i^j \tag{19}$$

and

$$\partial_t^{i,j}\omega_i^j + \partial_x^{i,j}\kappa_i^j = 0, \tag{20}$$

where $f_i^j = f(x_i, t_j)$, and $\partial_t^{i,j}$ and $\partial_x^{i,j}$ are discretizations of the corresponding derivatives ∂_t and ∂_x, then the numerical scheme (19) is said to be multisymplectic if (20) is a discrete conservation law of (19).

A standard method for constructing multisymplectic schemes is to apply a known symplectic discretization to each independent variable. For example, applying the symplectic midpoint rule (the lowest order member of the Gauss–Legendre family of schemes) to both the time and space derivatives in (1) yields a MS "centered cell" discretization [3]

$$\boldsymbol{M}\left(\frac{z_{1/2}^{1}-z_{1/2}^{0}}{\Delta t}\right)+\boldsymbol{K}\left(\frac{z_{1}^{1/2}-z_{0}^{1/2}}{\Delta x}\right)=\nabla_{z}S(z_{1/2}^{1/2}), \tag{21}$$

where we use the notation

$$z_{1/2}^{j}=\frac{1}{2}\left(z_{0}^{j}+z_{1}^{j}\right),\quad z_{i}^{1/2}=\frac{1}{2}\left(z_{i}^{0}+z_{i}^{1}\right),\quad z_{1/2}^{1/2}=\frac{1}{4}(z_{0}^{0}+z_{0}^{1}+z_{1}^{0}+z_{1}^{1}). \tag{22}$$

Multisymplecticity of scheme (21) is easily established. Associated with (21) is the discrete variational equation

$$\boldsymbol{M}\left(\frac{\mathrm{d}z_{1/2}^{1}-\mathrm{d}z_{1/2}^{0}}{\Delta t}\right)+\boldsymbol{K}\left(\frac{\mathrm{d}z_{1}^{1/2}-\mathrm{d}z_{0}^{1/2}}{\Delta x}\right)=\boldsymbol{S}_{zz}\,\mathrm{d}z_{1/2}^{1/2}. \tag{23}$$

Taking the wedge product of $\mathrm{d}z_{1/2}^{1/2}$ with (23), note that the right-hand side is zero since $\boldsymbol{S}_{zz}$ is symmetric. The terms on the left-hand side can be simplified

$$\begin{aligned}\mathrm{d}z_{1/2}^{1/2}\wedge\boldsymbol{M}(\mathrm{d}z_{1/2}^{1}-\mathrm{d}z_{1/2}^{0})&=\frac{1}{2}(\mathrm{d}z_{1/2}^{1}+\mathrm{d}z_{1/2}^{0})\wedge\boldsymbol{M}(\mathrm{d}z_{1/2}^{1}-\mathrm{d}z_{1/2}^{0})=\frac{1}{2}(\mathrm{d}z_{1/2}^{1}\wedge\boldsymbol{M}\,\mathrm{d}z_{1/2}^{1}-\mathrm{d}z_{1/2}^{0}\wedge\boldsymbol{M}\,\mathrm{d}z_{1/2}^{0})\\&=\omega_{1/2}^{1}-\omega_{1/2}^{0},\end{aligned}$$

whereas

$$\begin{aligned}\mathrm{d}z_{1/2}^{1/2}\wedge\boldsymbol{K}(\mathrm{d}z_{1}^{1/2}-\mathrm{d}z_{0}^{1/2})&=\frac{1}{2}(\mathrm{d}z_{1}^{1/2}+\mathrm{d}z_{0}^{1/2})\wedge\boldsymbol{K}(\mathrm{d}z_{1}^{1/2}-\mathrm{d}z_{0}^{1/2})=\frac{1}{2}(\mathrm{d}z_{1}^{1/2}\wedge\boldsymbol{K}\,\mathrm{d}z_{1}^{1/2}-\mathrm{d}z_{0}^{1/2}\wedge\boldsymbol{K}\,\mathrm{d}z_{0}^{1/2})\\&=\kappa_{1}^{1/2}-\kappa_{0}^{1/2}.\end{aligned}$$

This implies that the numerical scheme (21) satisfies the discrete multisymplectic conservation law

$$\left(\frac{\omega_{1/2}^{1}-\omega_{1/2}^{0}}{\Delta t}\right)+\left(\frac{\kappa_{1}^{1/2}-\kappa_{0}^{1/2}}{\Delta x}\right)=0.$$

3.1. The MS-CC discretization for the nonlinear Schrödinger equation

Applying the centered-cell discretization to the NLS system (7), we obtain the following multisymplectic scheme:

$$\begin{aligned}&\frac{q_{1/2}^{1}-q_{1/2}^{0}}{\Delta t}-\frac{v_{1}^{1/2}-v_{0}^{1/2}}{\Delta x}=2[(p_{1/2}^{1/2})^{2}+(q_{1/2}^{1/2})^{2}]p_{1/2}^{1/2},\\&-\frac{p_{1/2}^{1}-p_{1/2}^{0}}{\Delta t}-\frac{w_{1}^{1/2}-w_{0}^{1/2}}{\Delta x}=2[(p_{1/2}^{1/2})^{2}+(q_{1/2}^{1/2})^{2}]q_{1/2}^{1/2},\\&\frac{p_{1}^{1/2}-p_{0}^{1/2}}{\Delta x}=v_{1/2}^{1/2},\\&\frac{q_{1}^{1/2}-q_{0}^{1/2}}{\Delta x}=w_{1/2}^{1/2}.\end{aligned}$$

Eliminating v and w, and recombining into a single complex equation (as before with $u=p+\mathrm{i}q$) we obtain the six-point difference scheme for the NLS equation

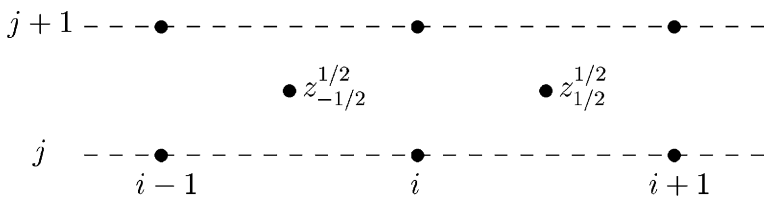

Fig. 1. MS-CC stencil.

$$\mathrm{i}(u^1_{-1/2}+u^1_{1/2}-u^0_{-1/2}-u^0_{1/2})/\Delta t+2(u^{1/2}_{-1}-2u^{1/2}_0+u^{1/2}_1)/\Delta x^2+2|u^{1/2}_{-1/2}|^2u^{1/2}_{-1/2}+2|u^{1/2}_{1/2}|^2u^{1/2}_{1/2}=0, \tag{24}$$

corresponding to the six-point stencil in Fig. 1 [10]. We designate this scheme MS-CC. Higher order multisymplectic schemes for the NLS equation can be obtained by concatenating higher order members in the Gauss–Legendre family of schemes [10].

3.1.1. Discrete conservation laws

A discrete form of the local conservation laws is obtained by applying the centered-cell discretization to (8) and (9). The residuals in the conservation laws are of the form

$$R^{1/2}_{1/2}=\frac{E^1_{1/2}-E^0_{1/2}}{\Delta t}+\frac{F^{1/2}_1-F^{1/2}_0}{\Delta x}, \tag{25}$$

where notation (22) is being used. The residuals, in general, are not equal to zero. If $S(z)$ is a quadratic functional of z, namely $S(z)=\frac{1}{2}z^{\mathrm{T}}\boldsymbol{A}z$ ($\boldsymbol{A}$ symmetric), and z^j_i is a solution the MS-CC scheme (21), then the local conservation laws are conserved exactly [3]. In the present case, since the PDEs under consideration are nonlinear, the local energy and momentum conservation laws will not be preserved exactly. However, the numerical experiments show that the local conservation laws are preserved very well over long times.

In the numerical experiments, we solve (24) using an iteration scheme and compute the residuals (25) at each time step.

4. Multisymplectic spectral discretizations

When a higher spatial resolution is demanded by a particular problem, spectral discretizations provide better approximations than finite-difference discretizations. In this section we show that spectral discretizations yield another class of multisymplectic integrators with associated spectral local conservation laws.

4.1. Multisymplectic PDEs in Fourier space

We start by considering the *discrete* Fourier transform and its inverse given by

$$Z_k=\frac{1}{L}\int_{-L/2}^{L/2}z(x,t)\mathrm{e}^{-\theta_k x}\,\mathrm{d}x,\quad z=\sum_{k=-\infty}^{\infty}Z_k\mathrm{e}^{\theta_k x},\quad \theta_k=\frac{2\pi\mathrm{i}}{L}k. \tag{26}$$

Collecting the Z_k's into the vector $Z=(\ldots,Z_{-1},Z_0,Z_1,\ldots)$, these formulas hold for $Z\in l^2(\mathbb{Z})$ (the set of square-summable sequences) and $z\in L^2[-L/2,L/2]$ (the set of square-integrable functions on $[-L/2,L/2]$). Letting $\boldsymbol{\Theta}$ be the diagonal matrix with entries given by θ_k and applying (26) to Eq. (1) yields the infinite-dimensional system of ODEs [4]

$$\boldsymbol{M}\partial_t Z + \boldsymbol{K}\boldsymbol{\Theta} Z = \nabla_Z \bar{S}, \tag{27}$$

where

$$\bar{S} = \int_{-L/2}^{L/2} S\left(\sum_{k=-\infty}^{\infty} Z_k e^{\theta_k x}\right) \mathrm{d}x.$$

Eq. (27) can appropriately be called a multisymplectic spectral PDE as there exist associated multisymplectic and energy conservation laws in Fourier space

$$\partial_t \mathscr{W} + \boldsymbol{\Theta}\mathscr{K} = 0, \quad \partial_t \mathscr{E} + \boldsymbol{\Theta}\mathscr{F} = 0,$$

where $\mathscr{W}, \mathscr{K}, \mathscr{E}, \mathscr{F}$ are the discrete Fourier transforms of ω, κ, E, F, respectively.

4.2. The discrete Fourier transform and its differentiation matrix

We now consider the fully discretized Fourier transform on an N-point grid and show that it yields a multisymplectic discretization. For N complex discrete values of u, the discrete Fourier transform (DFT) and its inverse are defined by

$$U_k = \{\boldsymbol{F}(u)\}_k = \frac{1}{N}\sum_{j=-N/2}^{N/2-1} u_j \mathrm{e}^{-\theta_k x_j}, \tag{28}$$

$$u_j = \{\boldsymbol{F}^{-1}(U)\}_j = \sum_{k=-N/2}^{N/2-1} U_k \mathrm{e}^{\theta_k x_j}, \tag{29}$$

where $u_j = u(x_j)$, $x_j = j\Delta x$ and $\Delta x = L/N$. To approximate the derivative at the grid points, consider the symmetric extension of (29) [7]

$$u(x) = \sum_{k=-N/2+1}^{N/2-1} U_k \mathrm{e}^{\theta_k x} + U_{\pm N/2}\cos\frac{N\pi}{L}x \quad \forall x \in [-L/2, L/2],$$

where $U_{\pm N/2}$ (the *Nyquist* frequency) is viewed as containing equal contributions from both modes $N/2$ and $-N/2$. Then the derivative at the grid points is approximated by

$$u'_j = \{\boldsymbol{F}^{-1}\{\bar{\boldsymbol{\Theta}}\boldsymbol{F}(u)\}\}_j = \sum_{k=-N/2+1}^{N/2-1} \theta_k U_k \mathrm{e}^{\theta_k x_j}, \tag{30}$$

where $\bar{\boldsymbol{\Theta}}$ has a zero diagonal entry for the Nyquist frequency which does not contribute to the odd derivatives at the grid points.

To show that the spectral discretization given by Eqs. (28) and (30) provides a multisymplectic discretization, it is convenient to express (30) in terms of a differentiation matrix $\boldsymbol{D}$,

$$u' = \boldsymbol{D}u.$$

After some calculus, it is found that $\boldsymbol{D}$ is given by

$$D_{jk} = \begin{cases} (-1)^{j-k}\frac{\pi}{L}\cot\frac{\pi}{L}(x_j - x_k) & \text{if } j \neq k, \\ 0 & \text{if } j = k. \end{cases} \tag{31}$$

Notice that $\boldsymbol{D}$ is a skew-symmetric matrix. Using the differentiation matrix (31), the multisymplectic equation (1) becomes

$$\boldsymbol{M}z_t + \boldsymbol{K}\boldsymbol{D}z = \nabla_z S. \tag{32}$$

Furthermore, $\boldsymbol{D}$ and $\boldsymbol{K}$ commute in the following sense:

$$\boldsymbol{K}\boldsymbol{D}z = \begin{pmatrix} K_{11} & \cdots & K_{1d} \\ \vdots & & \vdots \\ K_{d1} & \cdots & K_{dd} \end{pmatrix} \begin{pmatrix} \boldsymbol{D}z_1 \\ \vdots \\ \boldsymbol{D}z_d \end{pmatrix} = \begin{pmatrix} K_{11}\boldsymbol{D}z_1 + & \cdots & +K_{1d}\boldsymbol{D}z_d \\ & \vdots & \\ K_{d1}\boldsymbol{D}z_1 + & \cdots & +K_{dd}\boldsymbol{D}z_d \end{pmatrix} \tag{33}$$

$$= \begin{pmatrix} \boldsymbol{D}(K_{11}z_1 + \cdots + K_{1d}z_d) \\ \vdots \\ \boldsymbol{D}(K_{d1}z_1 + \cdots + K_{dd}z_d) \end{pmatrix} = \begin{pmatrix} \boldsymbol{D}(\boldsymbol{K}z)_1 \\ \vdots \\ \boldsymbol{D}(\boldsymbol{K}z)_d \end{pmatrix} = \boldsymbol{D}\boldsymbol{K}z. \tag{34}$$

It is now straightforward to prove that a discretization based on the discrete Fourier transform is multisymplectic. Taking the wedge product of $\mathrm{d}z$ with the associated variational equation, $\boldsymbol{M}\,\mathrm{d}z_t + \boldsymbol{K}\boldsymbol{D}\,\mathrm{d}z = \boldsymbol{S}_{zz}\,\mathrm{d}z$, yields

$$(\mathrm{d}z \wedge \boldsymbol{M}\,\mathrm{d}z)_t + \boldsymbol{D}\,\mathrm{d}z \wedge \boldsymbol{K}\mathrm{d}z + \mathrm{d}z \wedge \boldsymbol{K}\boldsymbol{D}\,\mathrm{d}z = 0, \tag{35}$$

which is a spectral discretization of the multisymplectic conservation law (4). Thus the DFT preserves the multisymplectic structure of the PDE (1).

4.3. Conservation of total symplecticity

The skew-symmetry of $\boldsymbol{D}$ provides another important invariant. Let the two forms ω_j and κ_{jk} be defined by

$$\omega_j = \frac{1}{2}\mathrm{d}z_j \wedge \boldsymbol{M}\,\mathrm{d}z_j \quad \text{and} \quad \kappa_{jk} = \frac{1}{2}(\mathrm{d}z_j \wedge \boldsymbol{K}\,\mathrm{d}z_k + \mathrm{d}z_k \wedge \boldsymbol{K}\,\mathrm{d}z_j).$$

Then we find that the discrete multisymplectic conservation law (35) is given by

$$\partial_t \omega_j + \sum_{k=0}^{N-1} D_{jk}\kappa_{jk} = 0.$$

Since $D_{jk} = -D_{kj}$ and $\kappa_{jk} = \kappa_{kj}$, summing over the spatial index, we arrive at the result

$$\partial_t \sum_{j=0}^{N-1} \omega_j = 0,$$

which implies that in addition to conservation of local symplecticity, we also have conservation of *total* symplecticity in time. This observation partially explains the superior performance of multisymplectic spectral discretizations in the numerical experiments.

4.4. The discrete local conservation laws

A fully multisymplectic spectral scheme is obtained by using a midpoint rule integration in time

$$\boldsymbol{M}\frac{z^1 - z^0}{\Delta t} + \boldsymbol{K}\boldsymbol{D}z^{1/2} = \nabla_z S(z^{1/2}). \tag{36}$$

In this case the residuals in the local conservation laws assume the form

$$R^{1/2} = \frac{E^1 - E^0}{\Delta t} + \boldsymbol{D}F^{1/2}. \tag{37}$$

It was observed that if $S(z)$ is a quadratic functional in z, then the MS-CC scheme conserves the LCLs exactly. We obtain a similar result for the MS-S scheme.

Theorem 1. *If $S(z)$ is quadratic in z, $S(z) = \frac{1}{2} z^T \boldsymbol{A} z$ ($\boldsymbol{A}$ symmetric), the MS-S scheme (36) conserves the local energy and momentum conservation laws exactly.*

Proof. Since $\boldsymbol{M}$ is skew-symmetric and $\boldsymbol{A}$ is symmetric, taking the inner product of (36) with $z^1 - z^0$, yields

$$(z^1 - z^0)^{\mathrm{T}} \boldsymbol{K}\boldsymbol{D}z^{1/2} = S(z^1) - S(z^0). \tag{38}$$

Similarly, since $\boldsymbol{K}$ is skew-symmetric, taking the inner product of (36) with $\boldsymbol{D}z^{1/2}$, we obtain

$$(\boldsymbol{D}z^{1/2})^{\mathrm{T}} \boldsymbol{M} \frac{z^1 - z^0}{\Delta t} = \boldsymbol{D}S(z^{1/2}). \tag{39}$$

Next, using (38) and the definitions (5) of E and F, we find that

$$\begin{aligned} \frac{E^1 - E^0}{\Delta t} + \boldsymbol{D}F^{1/2} &= \frac{S(z^1) - S(z^0) - \frac{1}{2} z^{1^T} \boldsymbol{K}\boldsymbol{D}z^1 + \frac{1}{2} z^{0^T} \boldsymbol{K}\boldsymbol{D}z^0}{\Delta t} + \boldsymbol{D}\left[\frac{1}{2} z^{1/2^T} \boldsymbol{K} \frac{z^1 - z^0}{\Delta t}\right] \\ &= \frac{1}{2\Delta t}\left[(z^1 - z^0)^{\mathrm{T}} \boldsymbol{K}\boldsymbol{D}z^{1/2} + \boldsymbol{D}z^{1/2^T} \boldsymbol{K}(z^1 - z^0)\right] = 0, \end{aligned}$$

which establishes discrete local conservation of energy.

Similarly, using (39) and definitions (5) of I and G, we obtain

$$\begin{aligned} \frac{I^1 - I^0}{\Delta t} + \boldsymbol{D}G^{1/2} &= \frac{\frac{1}{2} z^{1^T} \boldsymbol{M}\boldsymbol{D}z^1 - z^{0^T} \boldsymbol{M}\boldsymbol{D}z^0}{\Delta t} + \boldsymbol{D}S(z^{1/2}) - \boldsymbol{D}\left[\frac{1}{2} z^{1/2^T} \boldsymbol{M} \frac{z^1 - z^0}{\Delta t}\right] \\ &= \frac{1}{2\Delta t}\left[(z^1 - z^0)^{\mathrm{T}} \boldsymbol{M}\boldsymbol{D}z^{1/2} + \boldsymbol{D}z^{1/2^T} \boldsymbol{M}(z^1 - z^0)\right] = 0, \end{aligned}$$

which establishes discrete local conservation of momentum. □

4.5. The multisymplectic spectral discretization for the nonlinear Schrödinger equation

Applying the DFT (28)–(30) to the NLS equation (7) yields the system

$$\begin{aligned} &\partial_t Q_k - \theta_k V_k = \partial_{P_k} \bar{S}(U), \\ &-\partial_t P_k - \theta_k W_k = \partial_{Q_k} \bar{S}(U), \\ &\theta_k P_k = V_k, \\ &\theta_k Q_k = W_k, \end{aligned} \tag{40}$$

which, after taking the inverse DFT, can be recombined into a single equation as

$$u_t - \mathrm{i}\boldsymbol{F}^{-1}\{\boldsymbol{\Theta}^2 \boldsymbol{F}(u)\} = 2\mathrm{i}|u|^2 u, \tag{41}$$

where $\boldsymbol{\Theta}$ is the truncated diagonal matrix with entries θ_k and $u = p + \mathrm{i}q$.

To obtain a fully multisymplectic discretization for the NLS equation, we discretize (41) in time using the second-order symplectic implicit midpoint rule. Let u^0 be the current value and u^1 the new value to be found after one time step. Then the multisymplectic spectral discretization of the NLS equation is given by

$$\frac{u^1 - u^0}{\Delta t} - \mathrm{i}\boldsymbol{F}^{-1}\{\boldsymbol{\Theta}^2\boldsymbol{F}(u^{1/2})\} = 2\mathrm{i}|u^{1/2}|^2 u^{1/2}, \tag{42}$$

with corresponding residuals in the local energy and momentum conservation laws of the form

$$R^{1/2} = \frac{E^1 - E^0}{\Delta t} + \boldsymbol{F}^{-1}\{\bar{\boldsymbol{\Theta}}\boldsymbol{F}(F^{1/2})\}. \tag{43}$$

The residuals in the local conservation laws (43) are monitored in the numerical experiments. We solve (41) with an iteration scheme and compute the local residuals (43) at each time step.

4.6. The multisymplectic spectral discretization for the sine-Gordon equation

Similarly, applying the DFT to the SG equation (12) yields the system

$$\begin{aligned} &-\partial_t V_k + \theta_k W_k = \{\boldsymbol{F}(\sin u)\}_k, \\ &\partial_t U_k = V_k, \\ &-\theta_k U_k = -W_k, \end{aligned} \tag{44}$$

which can also be recombined into the single equation

$$\ddot{U}_k = -\theta_k^2 U_k - \{\boldsymbol{F}(\sin u)\}_k. \tag{45}$$

The separable Hamiltonian, $H = T + V$, associated with Eq. (45), allows us to use the general form of the explicit higher order symplectic integrators given by the following scheme [18]: let $u^0 = (p^0, q^0)$ be the current solution; set $(a_0, b_0) = (p^0, q^0)$ and

$$\begin{aligned} a_i &= a_{i-1} - \mathrm{d}t\, C_i V'(b_{i-1}), \\ b_i &= b_{i-1} + \mathrm{d}t\, D_i T'(a_i), \quad i = 1, \ldots, m. \end{aligned} \tag{46}$$

Then the solution after one time step is given by $u^1 = (p^1, q^1) = (a_m, b_m)$. The coefficients C_i and D_i are chosen so that the scheme is symplectic and of order $\mathcal{O}(\mathrm{d}t^m)$. For example, a first- and second-order schemes are given by choosing $m = 1$, $C_1 = D_1 = 1$ and $m = 2$, $C_1 = 0$, $C_2 = 1$, $D_1 = D_2 = \frac{1}{2}$, respectively. A fourth-order scheme, S_4, can be obtained by forming the following product of second-order integrators S_2:

$$S_4(\mathrm{d}t) = S_2(\beta\,\mathrm{d}t)\, S_2(\alpha\,\mathrm{d}t)\, S_2(\beta\,\mathrm{d}t), \tag{47}$$

where $\alpha = -2^{1/3}\beta$ and $\beta = 1/(2 - 2^{1/3})$. In the numerical experiments the second- and fourth-order schemes are denoted S-SY2 and S-SY4, respectively.

5. Numerical results

To test the performance of the various multisymplectic methods, we solve the NLS and SG equations with periodic boundary conditions $u(x + L, t) = u(x, t)$ over the time interval $[0, T]$. We begin in Section 5.1

by discussing the preservation of the local conservation laws and the leading constants of motion $\mathscr{E}(t)$, $\mathscr{I}(t)$ and $\mathscr{N}(t)$. In Section 5.2 we investigate the preservation of phase space structure by multisymplectic discretizations.

5.1. Preservation of local and global conservation laws

For the NLS equation we use initial conditions of the form

$$u_0(x) = a(1 + \epsilon \cos \mu x), \tag{48}$$

where $a = 0.5$, $\epsilon = 0.1$, $\mu = 2\pi/L$, and L is chosen to excite either (a) one mode ($L = 2\sqrt{2}\pi$) or (b) two modes ($L = 4\sqrt{2}\pi$). These initial conditions correspond to a perturbation of the spatially uniform plane wave. The resulting perturbed spatial profile corresponds to a multi-phase quasi-periodic (in time) solution of the NLS equation.

Fig. 2 provides the results obtained using MS-CC, Eq. (24), for initial data (48a), with $N = 32$ and $\Delta t = 10^{-3}$, over the time interval $T = 1000$. For clarity, in the plots we only show the time slice [950,1000]. The surface of the one mode multi-phase solution (Fig. 2(a)) exhibits quasiperiodic breather motion. Fig. 2(b)–(c) show the residuals in the local energy and momentum conservation law as given by (25). The residuals are concentrated in the regions of the multi-phase solution where there are steep gradients. The corresponding errors in the global energy and momentum over the time interval [950,1000] are given in Fig. 2(d)–(e). It is interesting to note that the global (i.e. after averaging over space) momentum and norm (not shown) are conserved exactly (up to the error criterion of 10^{-14} in the implementation of the scheme) since they are quadratic invariants. Additionally, the global (i.e. after averaging over time) energy flux is a quadratic invariant for the spatial symplectic scheme, and therefore is preserved over spatial path to machine accuracy (see Fig. 2(f)–(g)). Further, bounded oscillations in the errors in the local conservation laws and global invariants are observed since the multisymplectic schemes are also globally symplectic in time. These features make the MS-CC a very attractive scheme.

However, the MS-CC can have difficulty resolving the qualitative features of the waveform in highly sensitive regimes, where the proximity to unstable solutions is an important computational issue. Fig. 3 shows the results obtained using MS-CC for initial data (48b) in the two-mode regime, with $N = 64$, $\Delta t = 10^{-3}$ and $T = 100$. MS-CC produces qualitatively incorrect solutions, as can be observed in Fig. 3(a): instead of quasiperiodic breather motion, the numerical solution quickly develops a temporally chaotic solution (the onset of the numerically induced temporal chaos is observed at approximately $t = 25$). In this scenario temporal chaos is characterized by a random switching in time of the location of the spatial excitations in the waveform. (For the correct behavior see the solution obtained with MS-S, Fig. 4). Fig. 3(b)–(c) show the residuals in the local energy and momentum conservation law as given by (25) and Fig. 3(c)–(d) show the errors in the global invariants. Surprisingly, despite the fact that MS-CC preserves the local conservation laws and the global invariants very well (the errors have bounded oscillations for the duration of the experiments), correct qualitative behavior in the waveform is not obtained.

Due to the high spatial resolution of the scheme, there are many advantages to using the multisymplectic spectral method MS-S. Fig. 4 shows the error in the residuals (43), and global energy and momentum using MS-S, for initial data (48a) in the one-mode regime with $N = 32$, $\Delta t = 10^{-3}$, $T = 1000$. The surface of the wave profile obtained using MS-S is essentially identical to that of MS-CC (Fig. 2(a)) and is not shown. However, the residuals in the local conservation laws and the errors in the global invariants obtained using MS-S are several orders of magnitude smaller than the errors obtained with MS-CC. For example, the difference in the error in the local MCL is $\mathscr{O}(10^{-4})$ using the MS-CC scheme, whereas it is $\mathscr{O}(10^{-8})$ using the MS-S discretization. The global momentum and norm are conserved up to the accuracy of the MS-S

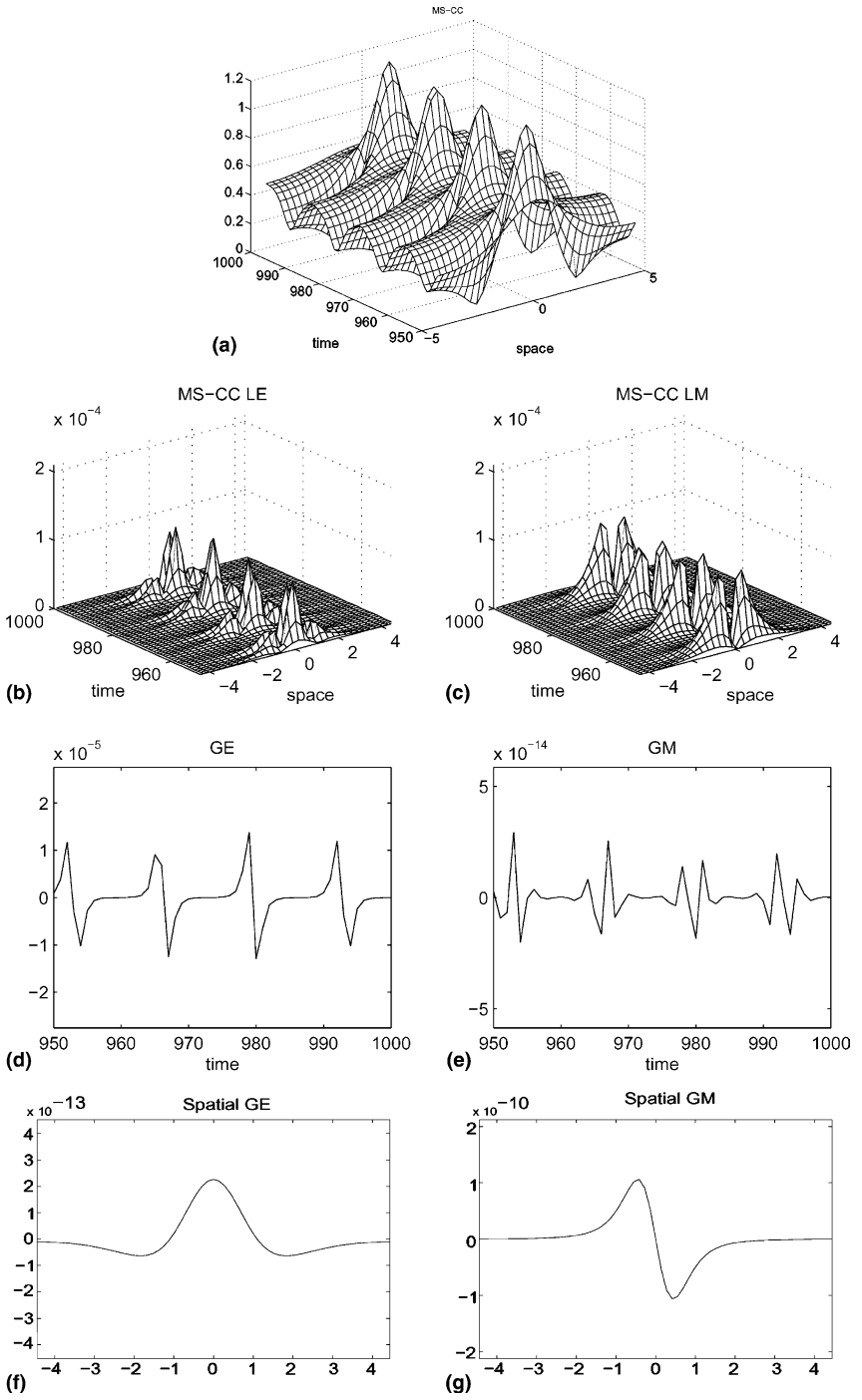

Fig. 2. The multisymplectic scheme MS-CC with $N = 32$, $\Delta t = 10^{-3}$ and $T = 1000$: (a) surface of the waveform; (b–c) error in the local energy and momentum conservation law, respectively, (d–e) error in the global energy and momentum, respectively, and (f–g) error in the spatial global energy and momentum, respectively, for initial data (48a).

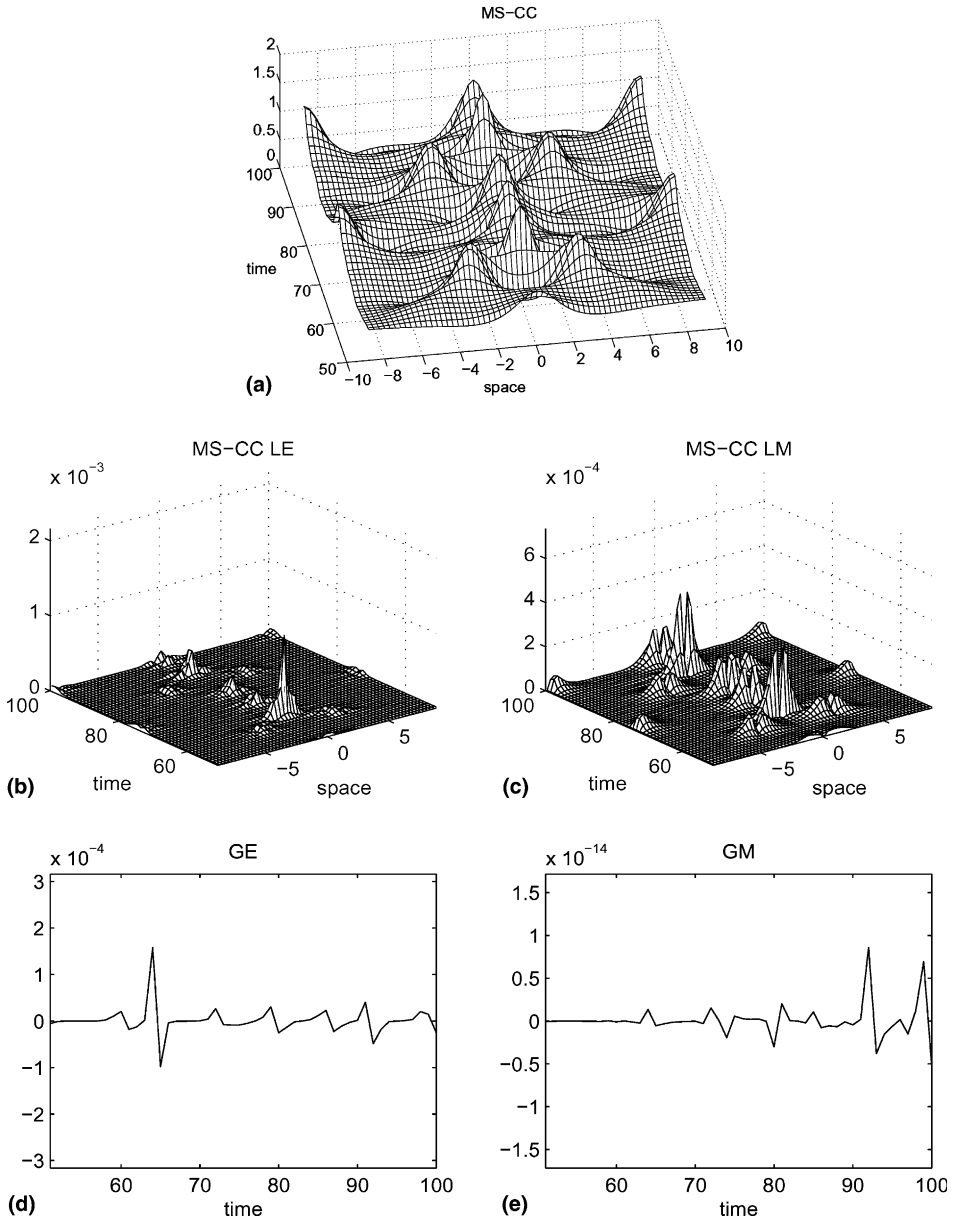

Fig. 3. The multisymplectic scheme MS-CC with $N = 64$, $\Delta t = 10^{-3}$ and $T = 100$: (a) surface of the waveform; (b–c) error in the local energy and momentum conservation law, respectively, and (d–e) error in the global energy and momentum, respectively, for initial data (48b).

scheme, supporting Theorem 1 on preservation of quadratic invariants. The errors in all the global invariants and local conservation laws oscillate and do not exhibit any growth for the duration of the simulation. It should be pointed out that although the errors obtained with MS-CC are larger, they exhibit no growth. The difference is due to the spatial accuracy of the schemes (i.e., spectral exponential accuracy vs finite-difference polynomial accuracy).

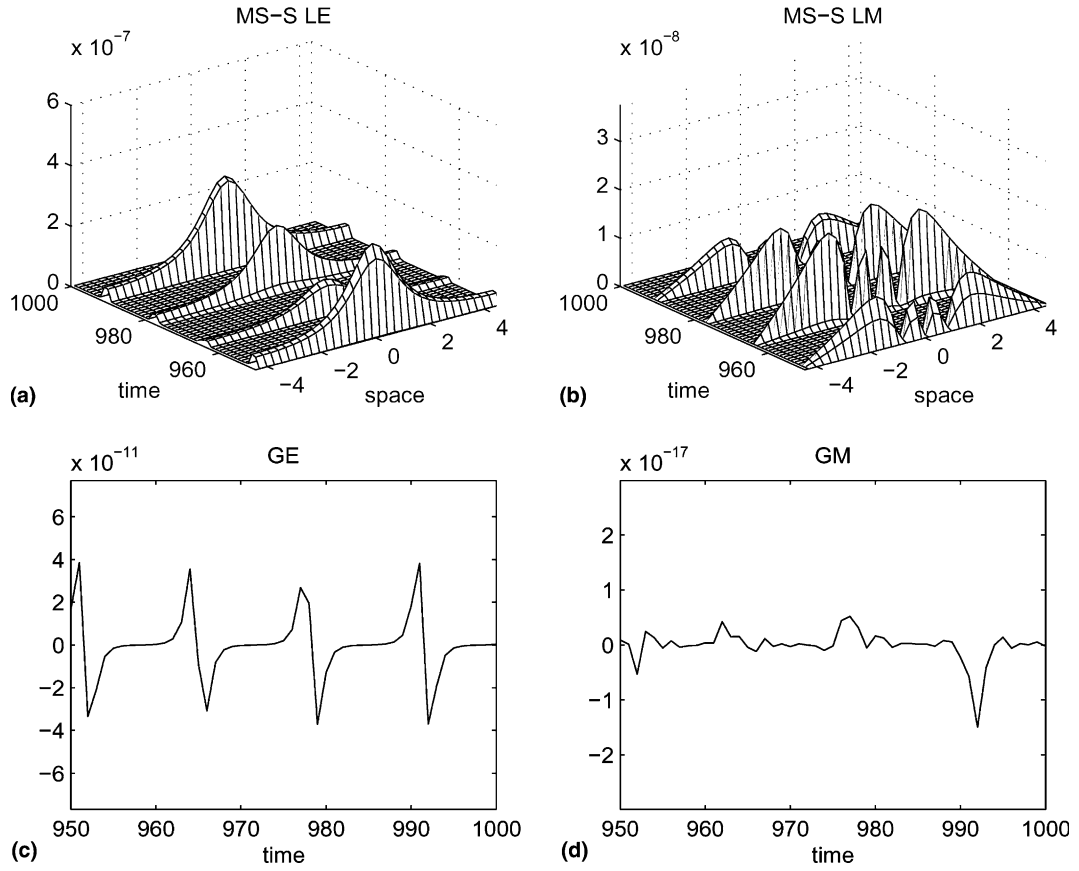

Fig. 4. The multisymplectic scheme MS-S with $N = 32$, $\Delta t = 10^{-3}$ and $T = 1000$: (a–b) error in the local energy and momentum conservation law, respectively, and (c–d) error in the global energy and momentum, respectively, for initial data (48a).

The importance of the local conservation laws (and in particular of the local MCL) as an indicator of spatial discretization errors which can corrupt the solution, is more clearly seen for solutions in the two-mode regime. As before, the errors in the local conservation laws (Fig. 5(b)–(c)) and global invariants (Fig. 5(d)–(e)) obtained with MS-S are several orders of magnitude smaller than with MS-CC. As a consequence, MS-S correctly resolves the quasi-periodic motion of multi-phase solutions. The MS-S scheme produces the correct quasi-periodic breather motion (Fig. 5(a)) for initial data (48b) in the two-mode regime with $N = 64$, $\Delta t = 10^{-3}$ and $T = 100$. Temporal irregularity and switching in the spatial excitations is not observed for the duration of the simulation, $0 < t < 100$. The global norm and momentum are conserved within roundoff by MS-S. The experiments suggest that preservation of the momentum conservation law is more sensitive to spatial refinement and to the complexity of the solution.

In the numerical experiments using MS-S we obtain very well resolved, high fidelity solutions. One question is whether the same results are obtained using a non-symplectic spectral method. That is, does specifically preserving multisymplecticity effect the qualitative properties of the numerical solution? Fig. 6 shows the errors in the residuals (43) and global invariants obtained using S-RK2, the non-symplectic (in time) and spectral (in space) scheme, for initial data (48a) with $N = 32$, $\Delta t = 10^{-3}$ and $T = 1000$. The most notable observation is that the errors in the LCLs and global invariants are growing and this growth is due to the non-symplectic time integrator. By $t = 850$, the time slice shown in Fig. 6, the errors in the local

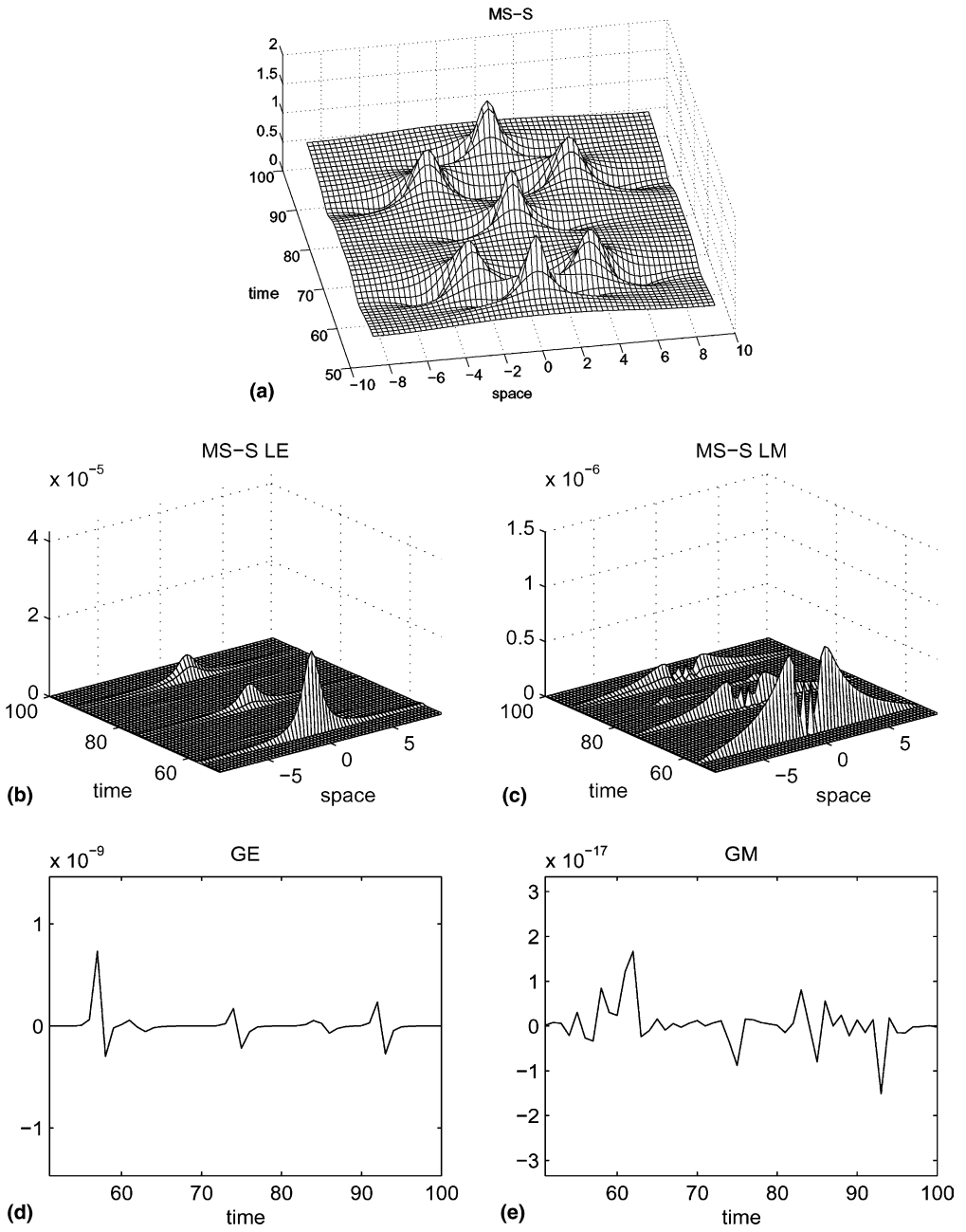

Fig. 5. The multisymplectic scheme MS-S with $N = 64$, $\Delta t = 10^{-3}$ and $T = 100$: (a) surface of the waveform; (b–c) error in the local energy and momentum conservation law, respectively, and (d–e) error in the global energy and momentum, respectively, for initial data (48b).

conservation laws and global invariants have grown to be *several* orders of magnitude larger than those obtained with MS-S (MS-S residuals exhibit oscillations which do not grow). Different combinations of N and Δt produce similar results.

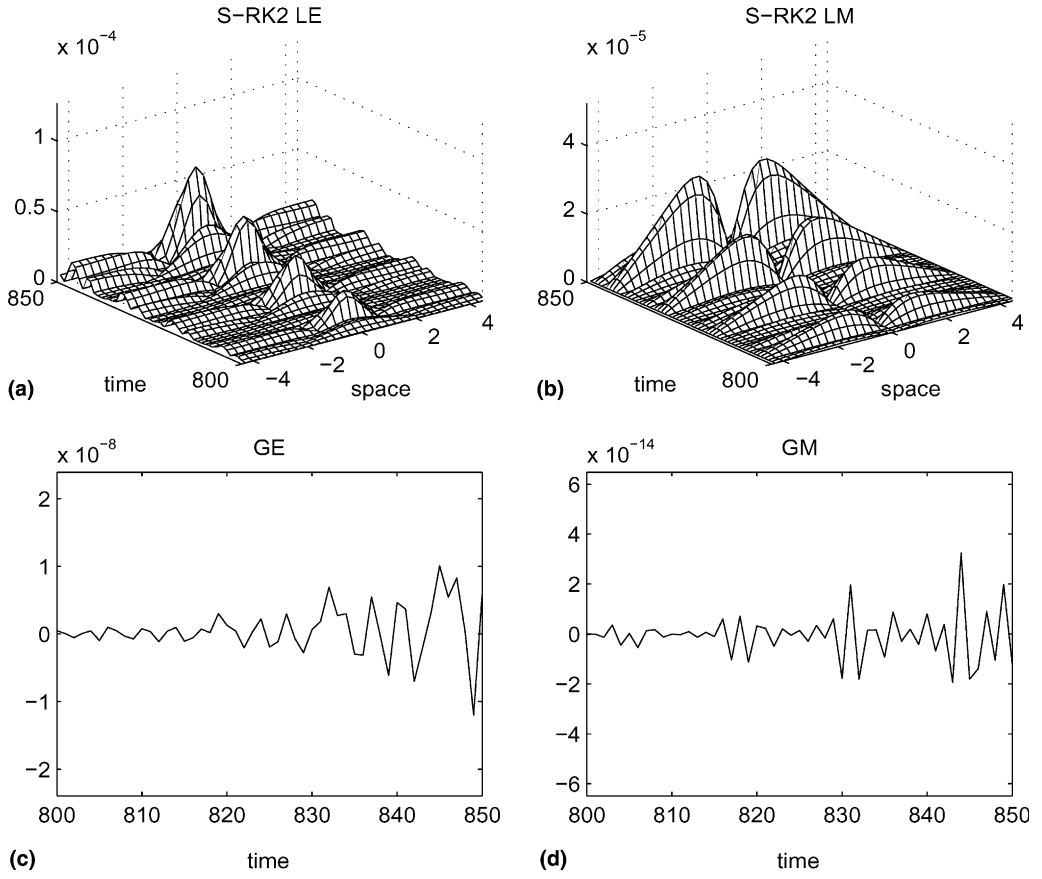

Fig. 6. The spectral scheme S-RK2 with $N = 32$, $\Delta t = 10^{-3}$ and $T = 1000$: (a–b) error in the local energy and momentum conservation law, respectively, and (c–d) error in the global energy and momentum, respectively, for initial data (48a).

5.2. Preservation of the phase space structure

Overall, the constants of motion and LCLS are remarkably well preserved by the MS-S scheme. Since we expect that the observed difference in resolution of the LCLs will be reflected in the long time global dynamics, we next study the preservation of phase space structures by MS-S and S-RK2. In other words, we investigate whether the multisymplectic property of a numerical scheme effects the scheme's ability to preserve phase space structures. To address this issue, we use the nonlinear spectrum (which incorporates all of the dynamical invariants and determines the phase space structure) as a basis for comparing the effectiveness of the integrators.

The NLS or SG spectrum is invariant. However, these equations are perturbed by the numerical truncation errors and the invariance of the spectrum is destroyed. We compute the spectral content of the initial data and monitor its evolution under the different numerical flows. It is not necessary to determine the entire Floquet spectrum $\sigma(\lambda)$; we are interested in only the periodic/antiperiodic eigenvalues, the roots of $\Delta \pm 2$. At each time t, we take the numerically generated solution $\{u_n(t) \,|\, n = 1, \ldots, N\}$ and perform the direct nonlinear spectral transform, i.e. the overdetermined system of ODEs (15) is numerically solved to obtain the discriminant Δ. The zero's of $\Delta \pm 2$ are then determined with a root solver which uses Muller's

method [15]. The schemes are evaluated in terms of how well the spectrum is resolved. The spectrum is computed with an accuracy on the order of $\mathcal{O}(10^{-8})$, whereas for the meshsizes and timesteps used in the numerical experiments, the numerical schemes are approximately $\mathcal{O}(10^{-6})$ accurate. Thus in the numerical experiments the spectrum is adequately resolved and the deviations in the spectrum are attributable to the numerical scheme.

We note here that since we are examining Fourier spectral discretizations, the most appropriate nonlinear spectral diagnostic to use is based on the Lax pair of the PDE. Integrable finite-difference discretizations of the NLS and SG do exist, with corresponding discrete Lax pairs. These discrete Lax pairs potentially provide alternative diagnostics that are more useful in studying the properties of finite-difference discretizations of the PDE.

5.2.1. The nonlinear Schrödinger equation

For the NLS equation we use (48a) which is initial data for a stable multiphase solution and the corresponding level sets are stable tori. This initial data is a small perturbation of the plane wave with one unstable mode, i.e. one complex double point in the spectrum. A perturbation analysis of the plane wave spectrum shows that for (48a) the primary spectrum is $\mathbb{R}$ along with a band-gap structure along the imaginary axis. (We only refer to elements of spectrum in the upper half plane since the spectrum is symmetric with respect to the real axis.) The end of the band of spectrum on the imaginary axis is given by λ_0. The complex double point has split into two simple points opening a gap (the width of which is determined by $|\lambda_1 - \lambda_2|$) in the spectrum [16]. All additional elements of the periodic spectrum, λ_i, correspond to stable inactive modes. We monitor the significant elements of the periodic spectrum λ_0, λ_1 and λ_2, along with the leading higher mode λ_3.

Fig. 7 provides the results obtained for initial data (48a) using MS-S (left column) and S-RK2 (right column) with $N = 32$, $\Delta t = 10^{-3}$ and $T = 850$. A comparison of the errors in the spectral elements λ_0, $|\lambda_1 - \lambda_2|$ and λ_3 is given, top to bottom. Note that the higher the mode, the less accurately it is resolved: using both schemes the error obtained in λ_0 is $\mathcal{O}(10^{-6})$, the error in $|\lambda_1 - \lambda_2|$ is $\mathcal{O}(10^{-5})$, and the error in λ_3 is $\mathcal{O}(10^{-4})$. However, we observe a qualitative difference in the results obtained with MS-S and S-RK2. The errors in λ_0 and $|\lambda_1 - \lambda_2|$ due to S-RK2 exhibit a linear drift that is typical of non-symplectic integrators, which is not observed using MS-S. Examining the error in the higher radiation modes λ_i, there is no qualitative difference in the results obtained with MS-S and S-RK2 (on the timescale examined), as the comparison of the error in λ_3 illustrates.

For long time simulations, S-RK2 poorly preserves the two main components of the spectral configuration. Remarkably, the errors obtained with MS-S oscillate but do not grow. This is a significant qualitative difference in the ability of the schemes to preserve the spectrum and hence the phase space structure.

5.2.2. The sine-Gordon equation

For the SG (11), we use the following initial data:

$$u(x,0) = \pi + 0.1\cos(\mu x), \quad u_t(x,0) = 0$$

with parameters $\mu = 2\pi/L$ and $L = 2\sqrt{2}\pi$. This initial data is for solutions in the unstable regime as the zeroth double point remains closed, i.e. the initial data is *on* the level set containing the homoclinic manifold. (Closed double points cannot be preserved by the numerical schemes and in the following experiments one observes that the zeroth mode is immediately split into a gap state by the numerical scheme.)

Fig. 8 shows the spectral scheme (46) implemented in time with an explicit second-order Runge–Kutta (S-RK2) and with the symplectic midpoint integrator (S-SY2). We use $N = 32$ Fourier modes and a fixed time step $\Delta t = 10^{-2}$. These methods are exponentially accurate in space, which allows for a very accurate initial approximation of the spectral configuration. To interpret the plots of the errors in the spectrum, note

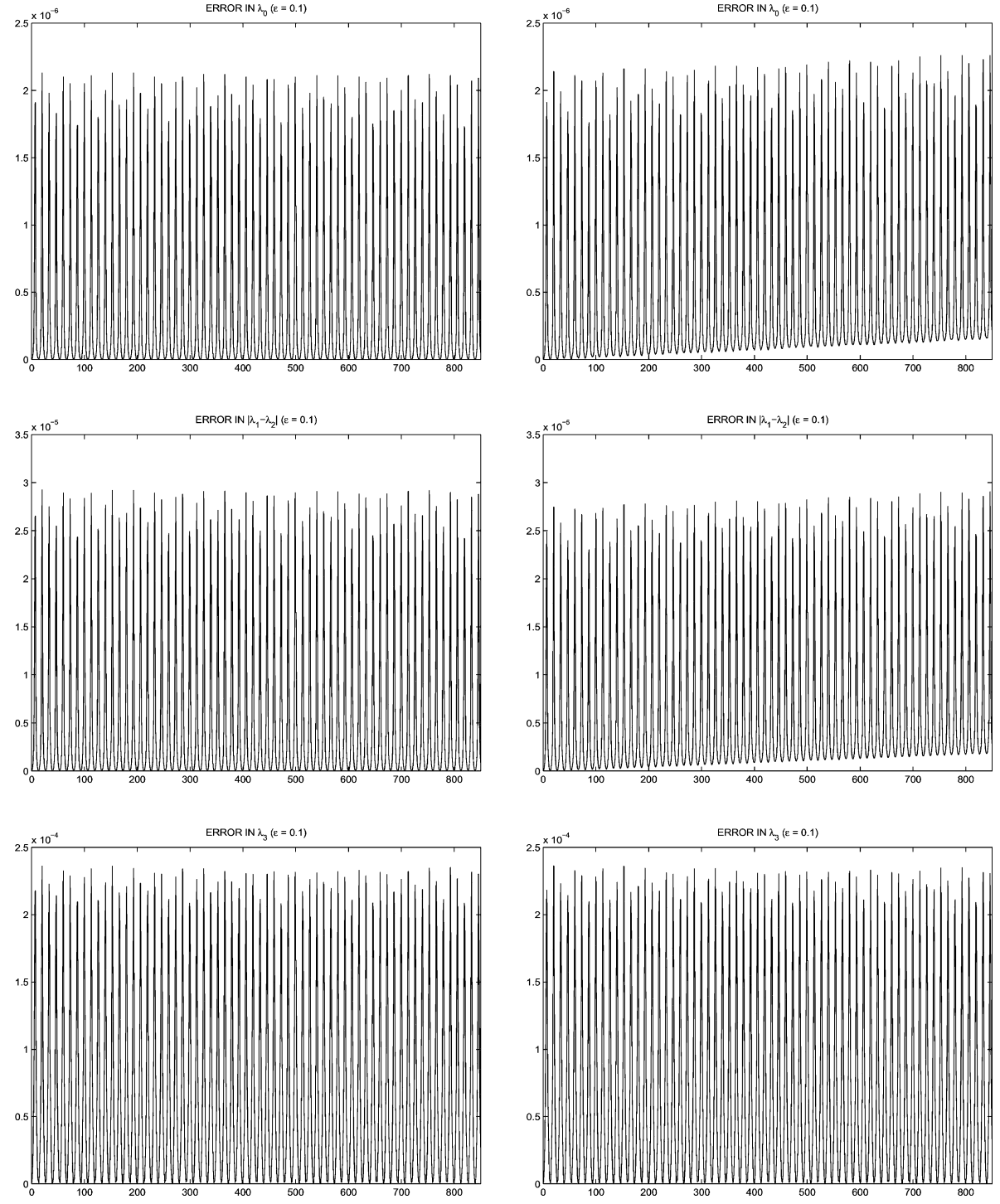

Fig. 7. Comparison of the error in λ_0, $|\lambda_1 - \lambda_2|$ and λ_3 obtained using MS-S (left column) and S-RK2 (right column) with $N = 32, \Delta t = 10^{-3}$, for initial data (48a).

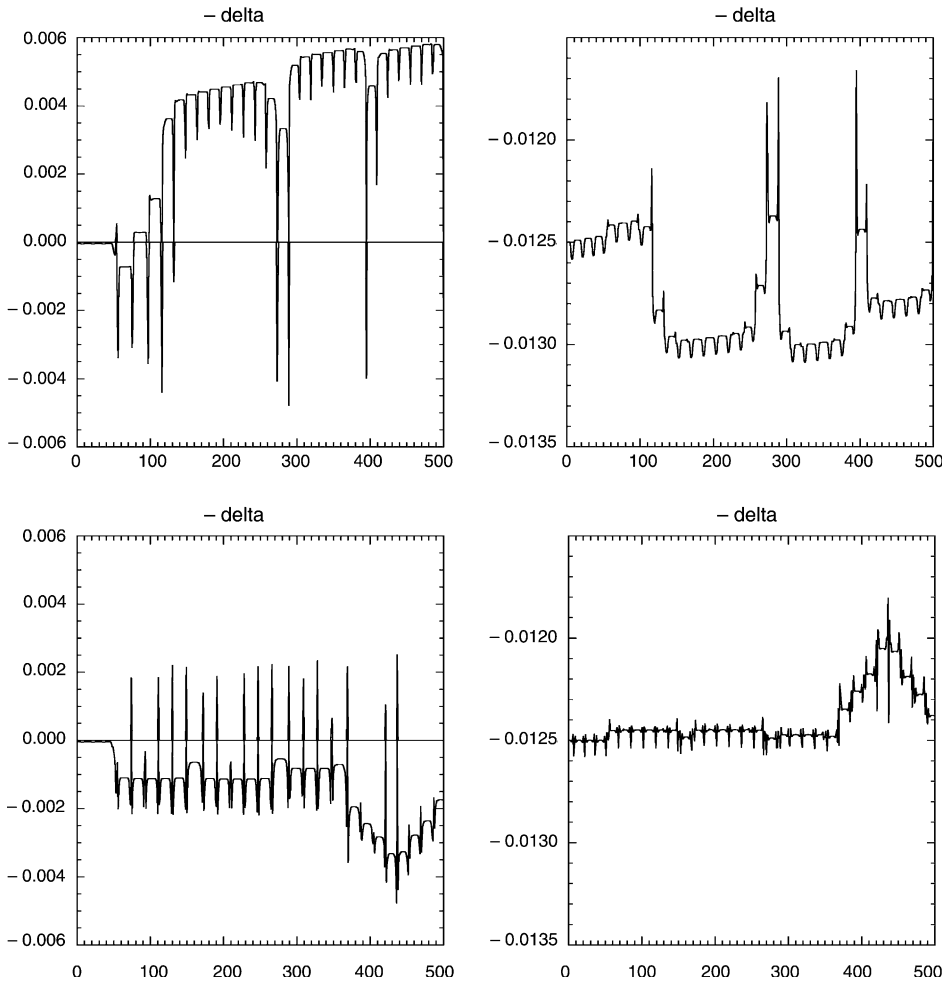

Fig. 8. Comparison of the error in $|\lambda_0 - \lambda_1|$ (left) and in $|\lambda_2 - \lambda_3|$ (right) for $u(x,0) = \pi + 0.1\cos\mu x, u_t(x,0) = 0, N = 32, T = 500$. (top) S-RK2; (bottom) S-SY2.

that under the perturbation from the numerical discretization, the complex double points can split in two ways – either into a gap along an arc of the circle, or into a cross along the radius.

We show a signed measure of the splitting distance in the spectrum associated with the zeroth mode, or error in $|\lambda_0 - \lambda_1|$, as a function of time. Positive and negative values represent gap and cross states, respectively. When the splitting distance passes through zero, the double points coalesce and homoclinic crossings occur. Using S-RK2 and S-SY2 (Fig. 8), the zeroth mode does display homoclinic crossings, as is to be expected.

The main observation is that with the non-symplectic S-RK2 there is a $O(10^{-3})$ linear drift in the error in $|\lambda_0 - \lambda_1|$. The error in $|\lambda_0 - \lambda_1|$ is smaller with S-SY2 and further, it doesn't drift. *Bounded* oscillations are observed. For both schemes, drifting in the error of the gap width $|\lambda_2 - \lambda_3|$ (spectrum associated with the first mode), is not observed and is $\mathcal{O}(10^{-6})$ for $0 < t < 500$ and so the torus component is accurately preserved.

The drift in the nonlinear spectrum obtained with S-RK2 can be eliminated on the timescale $0 < t < 500$ by increasing the accuracy of the integrator and using fourth order symplectic, S-SY4, and non-symplectic, S-RK4, time implementations of the spectral scheme. In this case the nonlinear spectral deviations are $O(10^{-4})$ for both S-RK4 and S-SY4 (Fig. 9).

However, the drift is not eliminated. Fig. 10 shows the results for the time slice $10,000 \leqslant t \leqslant 10,500$, when using $N = 32$ and $\Delta t = 10^{-2}$. Using S-RK4, Fig. 10 shows that the error in $|\lambda_0 - \lambda_1|$ have drifted to about 1.2×10^{-4} whereas for S-SY4 it continues to oscillate about 5×10^{-5}. Since the initial data is chosen on the homoclinic manifold, it is to be expected that there will be a higher density of homoclinic crossings when the spectrum is more accurately preserved, as the numerical trajectory is trapped in a narrower band about the homoclinic manifold.

The results obtained in the SG study confirm our previous observations: the multisymplectic scheme MS-S preserves the phase space structures of interest more accurately than the non-symplectic schemes. Although the drift observed with non-symplectic schemes can be reduced by using a higher order

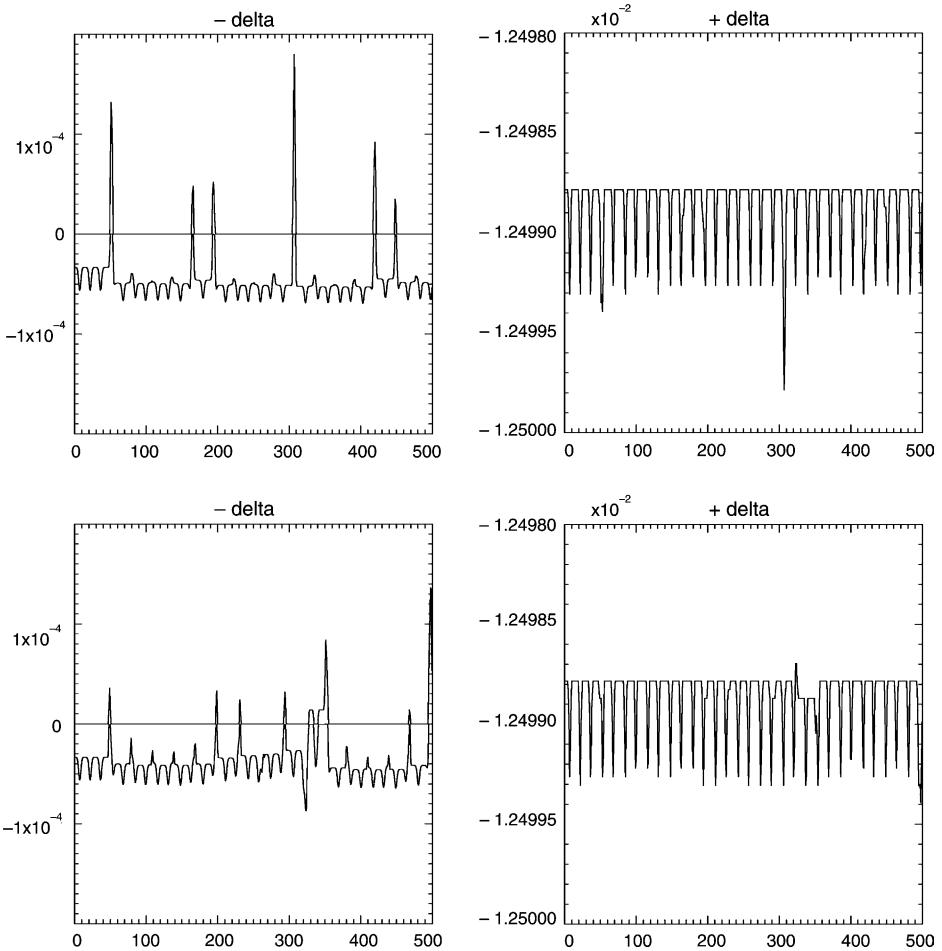

Fig. 9. Comparison of the error in $|\lambda_0 - \lambda_1|$ (left) and in $|\lambda_2 - \lambda_3|$ (right) for $u(x,0) = \pi + 0.1\cos\mu x$, $u_t(x,0) = 0$, $N = 32$, $T = 500$. (top) S-RK4; (bottom) S-SY4.

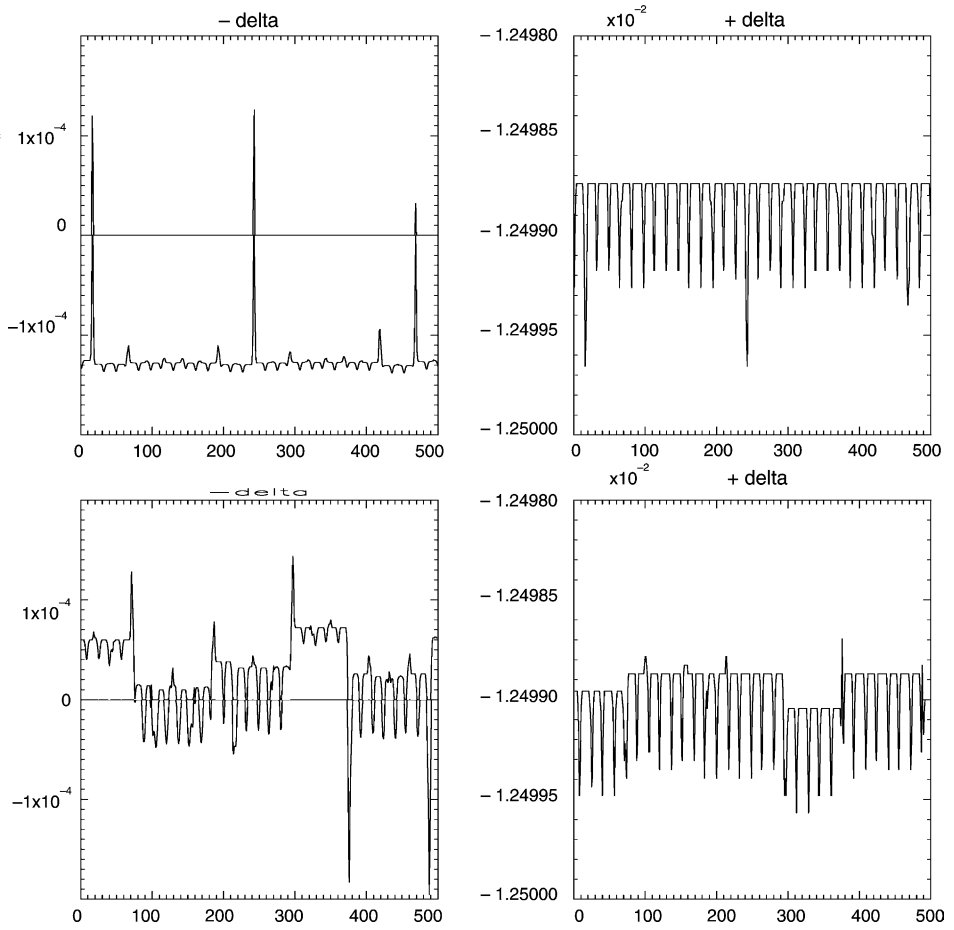

Fig. 10. Comparison of the error in $|\lambda_0 - \lambda_1|$ (left) and in $|\lambda_2 - \lambda_3|$ (right) for $u(x,0) = \pi + 0.1\cos\mu x$, $u_t(x,0) = 0$, $N = 32$, $T = 10,000$–$10,500$. (top) S-RK4; (bottom) S-SY4.

integrator, it is not eliminated and simply results in a poorer long-time preservation of the spectral configuration.

6. Conclusions

In this paper we have developed and examined the preservation properties of several multisymplectic integrators for the NLS and SG equations. We find that multisymplectic discretizations provide very efficient geometric integrators at reasonable computational costs. The numerical experiments indicate that the geometric features of the system are preserved better by the multisymplectic schemes than by traditional non-symplectic integrators. We find that the benefits of multisymplectic integrators include improved resolution of the local conservation laws, dynamical invariants and complicated phase space structures. This provides a deeper understanding of the local and global properties of MS integrators.

Further insight into the improved resolution of the local conservation laws by the MS schemes in the numerical experiments is obtained with backward error analysis, where one interprets the numerical so-

lution as a higher order solution of a modified PDE. For certain MS schemes it has been shown that the modified PDE is again multisymplectic [17]. In [11], we carry out a backward error analysis of the MS finite-difference discretization of the NLS equation and verify that the modified local conservation laws are preserved to higher order by the numerical solution. This further supports the use of MS integrators in long time numerical simulations of Hamiltonian PDEs.

Acknowledgements

This work was partially supported by the NSF, Grant No. DMS-0204714. The authors thank the referees for pointing out the Lagrangian approach for developing an improved multisymplectic form for the sine-Gordon equation.

References

[1] T.J. Bridges, Multisymplectic structures and wave propagation, Math. Proc. Cambridge Philos. Soc. 121 (1997) 147.
[2] T.J. Bridges, G. Derks, Unstable eigenvalues and the linearization about solitary waves and fronts with symmetry, Proc. Roy. Soc. London A 455 (1999) 2427.
[3] T.J. Bridges, S. Reich, Multisymplectic integrators: numerical schemes for hamiltonian pdes that conserve symplecticity, Phys. Lett. A 284 (2001) 184.
[4] T.J. Bridges, S. Reich, Multisymplectic spectral discretizations for the Zakharov–Kuznetsov and shallow water equations, Physica D 152 (2001) 491.
[5] N. Ercolani, D.W. McLaughlin, Toward a topological classification of integrable pde's, in: R. Devaney, H. Flaschka, W. Meyer, T. Ratiu (Eds.), Proceedings of the MSRI Workshop on Symplectic Geometry, 1990.
[6] L.D. Faddeev, L.A. Takhtajan, Hamiltonian Methods in the Theory of Solitons, Springer, Berlin, 1987.
[7] B. Fornberg, A Practical Guide to Pseudospectral Methods, Cambridge University Press, Cambridge, MA, 1998.
[8] E. Hairer, Ch. Lubich, G. Wanner, Geometric Numerical Integration, Springer, Berlin, 2002.
[9] J. Hong, Y. Liu, H. Munthe-Kaas, A. Zanna, On a multisymplectic scheme for Schrödinger equations with variable coefficients, 2003, preprint.
[10] A.L. Islas, D.A. Karpeev, C.M. Schober, Geometric integrators for the nonlinear Schrödinger equation, J. Comput. Phys. 173 (2001) 116.
[11] A.L. Islas, C.M. Schober, Backward error analysis for multisymplectic discretizations of Hamiltonian PDEs, Math. Comput. Simulation (2003), accepted.
[12] A.L. Islas, C.M. Schober, Multisymplectic spectral methods for the gross-pitaevski equation, Future Gener. Comput. Syst. 19 (2003) 403.
[13] D. Karpeev, C.M. Schober, Local Lagrangian formalism and discretization of the Heisenberg magnet model, Math. Comput. Simulation (2003), accepted.
[14] J.E. Marsden, S. Shkoller, Multisymplectic geometry, covariant Hamiltonians and water waves, Math. Proc. Cambridge Philos. Soc. 125 (1999) 553.
[15] D.W. McLaughlin, E.A. Overman, Whiskered Tori for integrable pdes and chaotic behavior in near integrable pdes, Surv. Appl. Math. 1 (1995) 83.
[16] D.W. McLaughlin, C.M. Schober, Chaotic and homoclinic behavior for numerical discretizations of the nonlinear Schrödinger equation, Physica D 57 (1992) 447.
[17] B. Moore, S. Reich, Multisymplectic integration methods for Hamiltonian pdes, Future Gener. Comput. Syst. 19 (2003) 395.
[18] H. Yoshida, Construction of higher order symplectic integrators, Phys. Lett. A 150 (1990) 262.